JACS
JOURNAL OF THE AMERICAN CHEMICAL SOCIETY

COMMUNICATION

pubs.acs.org/JACS

Identification of 5−7 Defects in a Copper Oxide Surface

Fan Yang, YongMan Choi, Ping Liu, Dario Stacchiola, Jan Hrbek, and José A. Rodriguez*

Chemistry Department, Brookhaven National Laboratory, Upton, New York 11973, United States

Supporting Information

ABSTRACT: A topological defect in a Cu_2O surface oxide grown on Cu(111) has been identified. Using scanning tunneling microscopy, we observed the formation of pentagonal and heptagonal rings within the Cu_2O surface oxide. These structures break the symmetry of the hexagonal oxide surface and are a consequence of the presence of oxygen vacancies in the Cu_2O surface. We propose that the pentagonal and heptagonal rings are formed through the rotation of a −O−Cu−O− chain in a manner similar to the Stone−Wales transformation. The proposed transformation is supported by the results of density functional theory calculations.

Many technical applications of metal oxides[1] are enabled through the presence of defects at oxide surfaces. It is now known that in catalysis, surface defects of metal oxides can not only tune the properties of supported metal nanoparticles[2] but also be involved directly as the active centers in chemical reactions.[3] In this communication, we report for the first time the identification of a topological defect that breaks symmetries at an oxide surface while maintaining the local stoichiometry of the surface metal oxide. This topological defect was observed in a surface of Cu_2O epitaxially grown on Cu(111). Unlike the typical hexagonal structure of Cu_2O(111), we observed the formation of pentagonal and heptagonal rings within the Cu_2O surface oxide on Cu(111).

Topological defects formed by the introduction of pentagonal and heptagonal rings into a hexagonal network (i.e., 5−7 defects) are well-known in carbon materials. These 5−7 defects, often called Stone−Wales (S−W) defects, play a central role in the formation of carbon nanotubes and tuning of their mechanical and electrical properties.[4] The formation of 5−7 defects has been observed in graphene[5] and carbon nanotubes,[6] where hexagons in the carbon network are transformed into heptagons and pentagons. The transformation mechanism, predicted by Stone and Wales[7] in 1986, involves a 90° in-plane rotation of two neighboring carbon atoms with respect to the midpoint of the C−C bond. Such a transformation has also been predicted for other sp^2-bonded materials, such as hexagonal boron nitride and polycyclic aromatic hydrocarbons.[8] In this communication, we show that an S−W-type transformation and 5−7 defects can also occur at the surface of non-sp^2-bonded materials, such as a copper oxide surface, where the bonds between atoms have a strong ionic character. Traditionally, defects are considered as a low-concentration component at the surface. For instance, in the surface of graphene, the 5−7 defects mainly appear at the grain boundaries and stitch graphene domains of different rotation into a sheet.[9] In a remarkable contrast, the 5−7 defects in the Cu_2O surface oxide can actually dominate the oxide phase of Cu_2O on Cu(111).

Understanding the chemical transformation and structural transition between copper and cuprous oxide (Cu_2O) is an outstanding issue generally associated with corrosion, catalysis, and microelectronics.[10] Studies of the initial oxidation process on a well-defined copper surface[11] started at the dawn of ultrahigh vacuum (UHV) surface science. An ordered ultrathin copper oxide layer could be formed by annealing the Cu(111) surface in 10^{-8}−10^{-5} Torr O_2 at elevated temperatures.[12−14] The structures of the copper oxide film closely resemble Cu_2O(111) and exist in two forms known as the "29" and "44" structures. Structural models for the "29" and "44" systems have been proposed by Jensen et al.[12] and Matsumoto et al.[13] Both suggest that the "29" and "44" structures originate from the distortion of a Cu_2O(111)-like layer. The Cu_2O(111)-like layer has the same hexagonal lattice as unreconstructed Cu_2O(111) except that the undercoordinated Cu atoms have been removed. In the studies mentioned above, the presence of a disordered copper oxide phase before the formation of the "44" or "29" structures was reported. However, it is unclear how the transition between the metallic copper and the Cu_2O surface oxide occurs. We show in the present study that the formation of ordered structures is in fact preceded by stages with phases that have local or long-range order. The experiments were carried out in an Omicron variable-temperature scanning tunneling microscopy (STM) system[15] with a base pressure of $<1 \times 10^{-10}$ mbar [for details, see the Supporting Information (SI)].

Summarized in Figure 1 are the intermediate structures observed during the oxidation of Cu(111) at 550 K to form the "44" Cu_2O surface oxide. Larger-scale STM images are presented in Figure S1 in the SI. The Cu_2O surface oxide grown on Cu(111) at >550 K displays a structure with local order (Figure 1b) that has some vacancies in comparison with an ideal Cu_2O(111) surface. Upon further exposure to O_2 (Figure 1c), an oxide phase with long-range order covers >90% of the copper terraces (marked in the white rectangle in Figure 1c). When the long-range-ordered oxide phase covers the whole surface, a transition occurs with the formation of a crystalline hexagonal oxide lattice occurs (Figure 1d). The ordered hexagonal lattice has a periodicity of 0.60 nm, corresponding to the lattice of the Cu_2O(111)-like layer. The observation of the hexagonal lattice provides direct evidence for the structure of the Cu_2O(111)-like layer postulated in previous studies.[12,13] Further oxidation of the ordered hexagonal oxide leads to the formation of the "44" Cu_2O surface oxide (not shown).

Received: May 20, 2011
Published: June 30, 2011

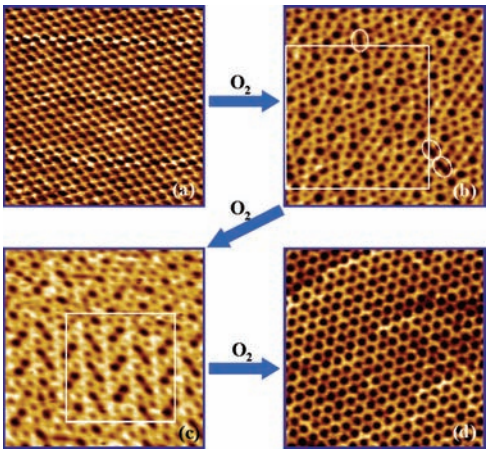

Figure 1. STM images of the intermediate structures of the Cu_2O surface oxide formed during oxidation of Cu(111) at 550 K: (a) Cu(111); (b) Cu_2O surface oxide with local order (~100 L O_2); (c) Cu_2O surface oxide showing regions with long-range order (~180 L O_2); (d) crystalline hexagonal Cu_2O surface oxide formed as the oxide phase covers the whole Cu(111) surface (~200 L O_2). White squares in (b) and (c) mark two areas that are illustrated in Figures 2 and 3, respectively. The dotted ellipses mark octagonal structures formed by the absence of a shared edge between two neighboring hexagons. Scan parameters: (a) −0.1 V, 1.4 nA; (b−d) −1.0 V, 0.1 nA. Image sizes: (a) 5 nm × 5 nm; (b−d) 10 nm × 10 nm.

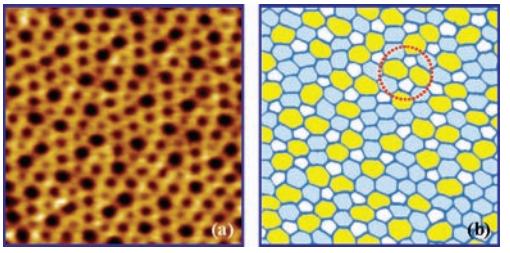

Figure 2. Structure of the Cu_2O surface oxide with local order. (a) Magnified STM image of the Cu_2O surface oxide in Figure 1b. (b) Schematic illustration of (a) with the pentagon, hexagon, and heptagon structures painted in white, yellow, and blue, respectively.

The structure of the Cu_2O surface oxide with local order is highlighted in Figure 2, which features a hexagonal layer intermixed with heptagons and pentagons. Not included are octagons that were also observed during the oxidation of Cu(111) (marked by dotted ellipses in Figure 1b and accounting for ~2% of the surface), which were caused by the absence of a −O−Cu−O− chain between neighboring hexagons (i.e., O vacancies). From Figure 2, it is also obvious that (1) the surface ratio of pentagons and heptagons is 1:1 and (2) pentagons and heptagons are always connected to each other. In Figure 2b, we have circled a unit with two heptagons and two pentagons connected to each other, termed as the pentagon−heptagon−heptagon−pentagon (5−7−7−5) structure.

As the Cu_2O surface oxide grows on Cu(111), the long-range order of the 5−7−7−5 structure starts to appear, as shown in Figure 1c and Figure 3. Within the regions showing long-range order, the pentagon/hexagon/heptagon number ratio becomes 1:1:1. Geometrically, the 5−7−7−5 structure draws an analogy

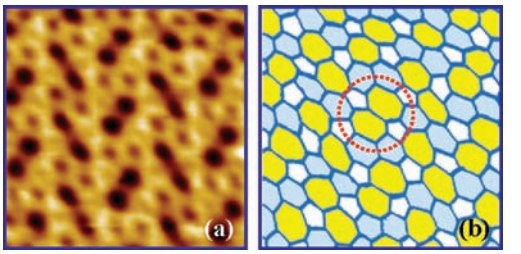

Figure 3. Cu_2O surface oxide showing regions with long-range order. (a) Magnified STM image of the Cu_2O surface oxide in the white square of Figure 1c. (b) Schematic illustration of (a) with the pentagon, hexagon, and heptagon structures painted in white, yellow, and blue, respectively.

with the S−W defects observed in carbon nanotubes and graphene layers. Therefore, we propose that the formation of a crystalline Cu_2O surface oxide might proceed via an S−W-type transformation of a "5−7" ordered structure, as shown in Figure 4.

To gain a better understanding of the S−W-type transformation of the Cu_2O surface oxide, we carried out density functional theory (DFT) calculations (for details, see the SI). The flat Cu(111) surface was simulated using a model involving a three-layer 8 × 8 slab with a vacuum space of 20 Å on which one atomic layer of Cu_2O surface oxide (36 Cu ions and 24 O ions) was deposited (Figure 4). The optimized geometries of the Cu_2O surface oxide before and after the S−W-type transformation are displayed in Figure 4. In the unit cell, there are 12 hexagons in the perfect structure (the hexagonal structure in our notation), while two pentagons, two heptagons, and eight hexagons are present in the defective structure, which contains two pentagon−heptagon (5−7) pairs (i.e., the 5−7−7−5 structure). The 5−7−7−5 structure was formed by twisting of a Cu−O−Cu moiety in the hexagonal structure by 90° to produce two 5−7 pairs while conserving the number of surface ions. Similar to the case of graphene,[16] our DFT calculations showed that the introduction of the 5−7−7−5 structure leads to a reconstruction of the Cu_2O network (Figure 4b). For the hexagonal structure, the oxygen ions of Cu_2O are sequentially distributed in a sequence as "O_U−O_L−O_U−O_L−O_U−O_L", where O_L and O_U represent oxygen atoms located at the lower and upper levels of the Cu_2O layer, respectively (Figure 4). However, because of the odd number of oxygen ions in the 5−7−7−5 structure, the topological defect breaks the alternating order. For instance, the heptagonal ring adopts an "O_L−O_U−O_L−O_U−O_L−O_U−O_U" or "O_U−O_L−O_U−O_L−O_U−O_L−O_L" sequence (Figure 4). The Cu−O distance between the Cu(111) and Cu_2O layers is significantly shorter in the "5−7" ordered oxide structure than in the crystalline hexagonal oxide structure (2.108 and 2.471 Å, respectively), indicating that the 5−7−7−5 structure has a stronger interaction with Cu(111) than the perfect hexagonal lattice. This is supported by a Bader charge calculation, which showed more electron transfer from the substrate to the Cu_2O layer in the 5−7−7−5 structure than in the hexagonal structure (charges of −3.2*e* and −3.0*e*, respectively). In other words, the defective 5−7−7−5 structure is stabilized by interactions with the Cu(111) surface. Indeed, our calculations showed that although the 5−7−7−5 structure is energetically less stable than the hexagonal structure, the corresponding difference in energy is only 0.53 eV per 5−7 pair.

In the STM experiments, the 5−7−7−5 structure was seen only when the system was not saturated with oxygen. Once the

dx.doi.org/10.1021/ja204652v | *J. Am. Chem. Soc.* 2011, 133, 11474–11477

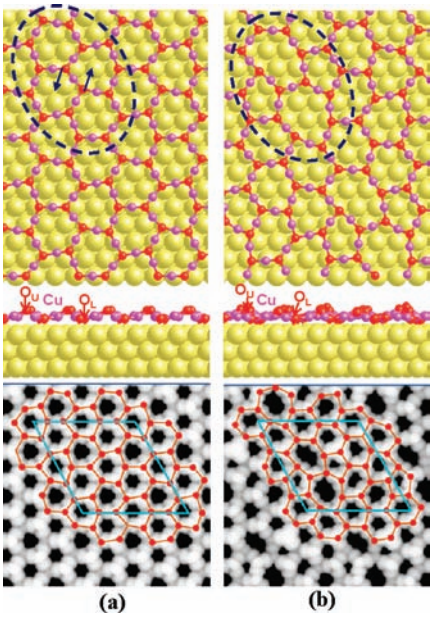

Figure 4. DFT calculations of the optimized structures of (a) the ordered hexagonal Cu_2O surface oxide and (b) the Cu_2O surface oxide including the 5−7−7−5 structure. The blue dashed ellipses mark (a) four neighboring hexagons and (b) the 5−7−7−5 structure after the S−W-type transformation. The black arrows in (a) illustrate the direction of rotation during an S−W-type transformation. The lower panels show simulated STM images of the above oxide at −1.0 V sample bias.

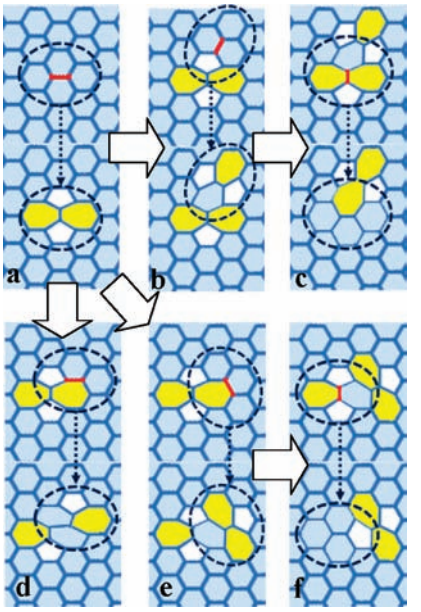

Figure 5. Modes of the S−W-type transformation. The −O−Cu−O− chains are represented by blue lines. In each panel, the upper and lower ellipses show the configuration before and after the S−W-type transformation, respectively. Red lines mark the −O−Cu−O− chain that rotates 90° during a transformation. The pentagons, hexagons, and heptagons are painted in white, yellow, and blue, respectively.

correct stoichiometry was reached for the whole Cu_2O overlayer, the ordered hexagonal lattice was seen in STM images. On the basis of the optimized structures, STM images[17] were also simulated by calculating the partial charge density with a −1.0 V bias, as shown in the lower panels of Figure 4. For clarity, polygons were superimposed on the simulated STM images. The simulated STM images for both the hexagonal network and the 5−7−7−5 structure agree well with the STM results.

An S−W-type transformation can explain the structure of the "5−7" Cu_2O surface oxide observed in our studies. Because of the limitation of computational resources, it was difficult to simulate the long-range order of the 5−7−7−5 structure or, on a larger scale, the local arrangement of the pentagonal and heptagonal structures. However, we were able to show that as long as the S−W-type transformation is a feasible mechanism, the pentagonal and heptagonal structures can be produced and populated within the ordered hexagonal lattice. Figure 5 illustrates the mechanism based on the S−W-type transformation. Basically, in each S−W-type transformation, there are four polygons involved. The four polygons can be a combination of pentagons, hexagons, and heptagons, which gives 15 possible combinations. When the transformation leading to the formation of octagons and triangles is excluded, there are only seven modes of S−W-type transformation left that could be involved in the phase transition of the Cu_2O surface oxide. The first two modes are the reversible transformation between four hexagons and the 5−7−7−5 structure (Figure 5a). The propagation of "5−7" pairs after the transformation of four hexagons into the 5−7−7−5 structure is illustrated in Figure 5b,e, which demonstrates transformations involving three hexagons and one pentagon/heptagon that lead to the formation of another "5−7" pair. On the basis of the modes in Figure 5a,b,e, the 5−7 defects could propagate along the surface in even or odd numbers. On the other hand, the annihilation of "5−7" pairs is illustrated in Figure 5c,f, where the transformations involve two pentagons/heptagons, one hexagon, and one heptagon/pentagon. On the basis of the modes in Figure 5c,f, the 5−7 defects could also rotate on the surface. As the transformation involves two hexagons and a "5−7" pair, Figure 5d illustrates the diffusion of a "5−7" pair by switching of its position with the two hexagons involved in the transformation.

Based on the modes illustrated in Figure 5, the structure of the "5−7" Cu_2O surface oxide could be produced from an ordered hexagonal lattice. Conversely, the ordered hexagonal oxide lattice could be produced from the "5−7" Cu_2O surface oxide. Figure 5 also shows that the S−W-type transformation would result in (1) a pentagon/heptagon ratio equal to 1 and (2) all of the pentagons and heptagons being connected to each other. Both results match exactly the two features that were observed in all of the "5−7" Cu_2O surface oxides. Moreover, Figure 5 shows that in order for the 5−7 defects to propagate, there must be three or four hexagons involved. This means that through the S−W-type transformation, the number of heptagons or pentagons would not increase further when the surface density of heptagons or pentagons equals that of the surrounding hexagons. This leads to a maximum surface concentration of 66.7% for the 5−7 defects (i.e., a pentagon/hexagon/pentagon ratio of 1:1:1). Indeed, in all of the "5−7" Cu_2O surface oxides observed in our studies, the concentration of the 5−7 defects was never larger than ∼66%. As the 5−7−7−5 structure arranges with long-range order (Figure 1c and 3), the surface concentrations of pentagons and heptagons reach their maximum values, giving a pentagon/hexagon/heptagon ratio of 1:1:1. Therefore, the S−W-type transformation explains all of the structures of the "5−7"

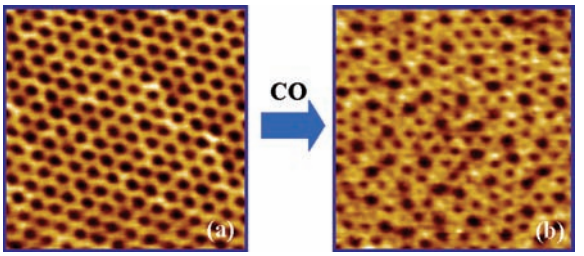

Figure 6. STM images of the intermediate structures of the Cu_2O surface oxide formed during the reduction of the "44" Cu_2O surface oxide on Cu(111) by CO at 800 K: (a) ordered Cu_2O surface oxide; (b) "5−7" Cu_2O surface oxide. Both images are 8 nm × 8 nm.

Cu_2O surface oxide observed in our studies. Since no Cu adatoms were observed during the phase transition of the Cu_2O surface oxide and in view of the mass conservation in a 2D system, the S−W-type transformation might be the only feasible mechanism to explain the phase transition in Cu_2O/Cu(111).

We also studied the reduction of the "44" Cu_2O surface oxide by CO (Figure 6).[15] We observed the transformation of the "44" structure into domains of the ordered hexagonal oxide phase (Figure 6a), which was eventually transformed into the "5−7" Cu_2O surface oxide (Figure 6b and SI) before being removed from the Cu(111) surface. Thus, the "5−7" Cu_2O surface oxide is present as an intermediate phase in both oxidation and reduction processes. Compared to the crystalline hexagonal Cu_2O surface oxide, the "5−7" Cu_2O surface oxide film is less saturated in oxygen overall because of the presence of vacancies and missing −O−Cu−O− chains within the oxide film and at the step edges.

The identification of 5−7 defects in the Cu_2O surface oxide on Cu(111) provides a new understanding of defects at oxide surfaces and shows that this type of structure is not a unique property of graphene, carbon nanotubes, and other types of sp^2-bonded materials. The existence of 5−7 defects in surfaces of Cu_2O can have an impact in catalysis, since the chemical and catalytic activity of this oxide is known to increase upon the generation of defects.[18] For example, Russell et al.[19] have established that in the partial oxidation of methanol catalyzed by Cu(111), the highest formaldehyde yield comes from the partially oxidized Cu(111) surface while the Cu(111) surface saturated with oxygen is not active. On the basis of their preparation conditions, the partially oxidized phase may correspond to the Cu_2O surface oxide dominated by 5−7 defects. With the identification of the 5−7 defects of the Cu_2O surface oxide, it is now necessary and interesting to revisit many copper-oxide-related catalytic processes and reaction mechanisms.

■ ASSOCIATED CONTENT

Supporting Information. Experimental and computational details and Figure S1. This material is available free of charge via the Internet at http://pubs.acs.org.

■ AUTHOR INFORMATION

Corresponding Author
rodrigez@bnl.gov

■ ACKNOWLEDGMENT

The authors thank the U.S. Department of Energy (Chemical Sciences Division, Grants DE-AC02-98CH10886 and DE-AC02-05CH11231) for financial support. DFT calculations were carried out at Center for Functional Nanomaterials at Brookhaven National Laboratory and the National Energy Research Scientific Computing (NERSC) Center. F.Y. is grateful to Huagen Yu for helpful discussions.

■ REFERENCES

(1) (a) Diebold, U. *Surf. Sci. Rep.* **2003**, *48*, 53. (b) Esch, F.; Fabris, S.; Zhou, L.; Montini, T.; Africh, C.; Fornasiero, P.; Comelli, G.; Rosei, R. *Science* **2005**, *309*, 752. (c) Kwak, J. H.; Hu, J. Z.; Mei, D.; Yi, C. W.; Kim, D. H.; Peden, C. H. F.; Allard, L. F.; Szanyi, J. *Science* **2009**, *325*, 1670. (d) Nilius, N. *Surf. Sci. Rep.* **2009**, *64*, 595.

(2) (a) Yan, Z.; Chinta, S.; Mohamed, A. A.; Fackler, J. P., Jr.; Goodman, D. W. *J. Am. Chem. Soc.* **2005**, *127*, 1604. (b) Santra, A. K.; Yang, F.; Goodman, D. W. *Surf. Sci.* **2004**, *548*, 324. (c) Schaub, R.; Thostrup, R.; Lopez, N.; Lægsgaard, E.; Stensgaard, I.; Nørskov, J. K.; Besenbacher, F. *Phys. Rev. Lett.* **2001**, *87*, No. 266104. (d) Chen, M. S.; Goodman, D. W. *Science* **2004**, *306*, 252.

(3) (a) Yang, F.; Graciani, J.; Evans, J.; Liu, P.; Hrbek, J.; Sanz, J. F.; Rodriguez, J. A. *J. Am. Chem. Soc.* **2011**, *133*, 3444. (b) Rodriguez, J. A.; Graciani, J.; Evans, J.; Park, J. B.; Yang, F.; Stacchiola, D.; Senanayake, S. D.; Ma, S. G.; Perez, M.; Liu, P.; Sanz, J. F.; Hrbek, J. *Angew. Chem., Int. Ed.* **2009**, *48*, 8047. (c) Rodriguez, J. A.; Ma, S.; Liu, P.; Hrbek, J.; Evans, J.; Perez, M. *Science* **2007**, *318*, 1757.

(4) Dekker, C. *Phys. Today* **1999**, *52*, 22.

(5) (a) Meyer, J. C.; Kisielowski, C.; Erni, R.; Rossell, M. D.; Crommie, M. F.; Zettl, A. *Nano Lett.* **2008**, *8*, 3582. (b) Hashimoto, A.; Suenaga, K.; Gloter, A.; Urita, K.; Iijima, S. *Nature* **2004**, *430*, 870.

(6) Suenaga, K.; Wakabayashi, H.; Koshino, M.; Sato, Y.; Urita, K.; Iijima, S. *Nat. Nanotechnol.* **2007**, *2*, 358.

(7) Stone, A. J.; Wales, D. J. *Chem. Phys. Lett.* **1986**, *128*, 501.

(8) (a) Bettinger, H. F.; Dumitricabreve, T.; Scuseria, G. E.; Yakobson, B. I. *Phys. Rev. B* **2002**, *65*, No. 041406. (b) Rabideau, P. W.; Sygula, A. *Acc. Chem. Res.* **1996**, *29*, 235.

(9) Huang, P. Y.; Ruiz-Vargas, C. S.; van der Zande, A. M.; Whitney, W. S.; Levendorf, M. P.; Kevek, J. W.; Garg, S.; Alden, J. S.; Hustedt, C. J.; Zhu, Y.; Park, J.; McEuen, P. L.; Muller, D. A. *Nature* **2011**, *469*, 389.

(10) (a) Paracchino, A.; Laporte, V.; Sivula, K.; Grätzel, M.; Thimsen, E. *Nat. Mater.* **2011**, *10*, 456. (b) Nian, J.-N.; Hu, C.-C.; Teng, H. *Int. J. Hydrogen Energy* **2008**, *33*, 2897. (c) Poizot, P.; Laruelle, S.; Grugeon, S.; Dupont, L.; Tarascon, J. M. *Nature* **2000**, *407*, 496.

(11) Ertl, G. *Surf. Sci.* **1967**, *6*, 208.

(12) (a) Jensen, F.; Besenbacher, F.; Stensgaard, I. *Surf. Sci.* **1992**, *270*, 400. (b) Jensen, F.; Besenbacher, F.; Lægsgaard, E.; Stensgaard, I. *Surf. Sci.* **1991**, *259*, L774.

(13) Matsumoto, T.; Bennett, R. A.; Stone, P.; Yamada, T.; Domen, K.; Bowker, M. *Surf. Sci.* **2001**, *471*, 225.

(14) Wiame, F.; Maurice, V.; Marcus, P. *Surf. Sci.* **2007**, *601*, 1193.

(15) Yang, F.; Choi, Y.; Liu, P.; Hrbek, J.; Rodriguez, J. A. *J. Phys. Chem. C* **2010**, *114*, 17042.

(16) Jeong, B. W.; Ihm, J.; Lee, G.-D. *Phys. Rev. B* **2008**, *78*, No. 165403.

(17) Tersoff, J.; Hamann, D. R. *Phys. Rev. B* **1985**, *31*, 805.

(18) (a) Pike, J.; Chan, S.-W.; Zhang, F.; Wang, X.; Hanson, J. *Appl. Catal., A* **2006**, *303*, 273. (b) White, B.; Yin, M.; Hall, A.; Le, D.; Stolbov, S.; Rahman, T.; Turro, N.; O'Brien, S. *Nano Lett.* **2006**, *6*, 2095.

(19) Russell, J. N., Jr.; Gates, S. M.; Yates, J. T., Jr. *Surf. Sci.* **1985**, *163*, 516.